Elementary numerical calculations on two-dimensional inverse scattering problems

P. P. Yu[1]

[1] *Department of Physics and Astronomy, Dartmouth College, 6127 Wilder Laboratory, Hanover, NH 03755 USA*

An optimized iterative algorithm for a particular type of inverse scattering problems is implemented in tendum with the method of boundary integral equations. Numerical examples show that with a decent initial guess the simple shape of the scatter in two dimensions can be obtained with sufficient satisfaction.

PACS numbers:

I. INTRODUCTION

The everlasting attention received by problems related to inverse scattering and target recognition has driven the field into an inflationary phase ever since their very emergence. A voluminous literature (published and confidential) on the subject makes a comprehensive up-to-date overview almost inconceivable. The intent of the present paper with limited extent is to study a particular algorithm of solving a two dimensional inverse scattering problem by adapting the method of boundary integral equations.

The statement of the problem is the following: Consider a two-dimensional solid obstacle of strictly convex and sufficiently smooth boundary in an otherwise spatially homogeneous unbounded region. The scattering of an incident monochromatic plane wave off the obstacle can be formulated as the solution to the exterior Dirichlet problem of the Helmholtz equation [1]. Assuming that one is accessible to the far-field pattern in terms of the angular power spectrum, the question is how to infer the shape of the obstacle.

Instead of attempting to harness more sophiscated algorithms, it is feasible to solve this problem, to a satisfactory degree, for a two-dimensinoal obstacle with simple shape by incorporating Fourier series together with appropriate search-optimization packages. The solver mainly consists of four steps: (0) Parametrize the boundary of the obstacle and represent it as a Fourier series whose coefficients constitute the vectors in a parameter space. (1) Guess an initial shape of the boundary by picking a starting point in the parameter space. (2) Apply boundary integral equations to obtain the far-field pattern and angular power spectrum by solving the exterior Dirichlet problem with the given boundary. (3) Compare the calculated spectrum with the measured one and minimize the error with an optimized iteration of minimum search over an assigned range in the parameter space until the genuine convergence is achieved. Typically, the convergence to true minimum depends heavily upon the initial guesses. It is ocassionally of significant help in accelerating the search if some knowledge of the dependence of the error function upon at least a partial set of the parameters is explored before the launch of a massive search with overly arbitrary initial guesses.

The structure of this article is as follows. Section II provides a quick recap of the method of boundary integral equations involved in solving the exterior Dirichlet problems. Section III is devoted to a complete presentation of the algorithm implemented in the solution of current inverse scattering problem. Numerical examples with explanations are included in Section IV. A summary and discussions are wrapped together in Section V.

II. BOUNDARY INTEGRAL EQUATIONS AND EXTERIOR DIRICHLET PROBLEMS

Solutions to exterior Dirichlet problems of the Helmholtz equation using boundary integral equations have been well documented in numerous literatures (e.g. [1]). For the sake of completeness, some major results that are closely related to the discussions in the following sections are briefly summarized here for references.

Let $D_- \subset \mathbf{R}^m$, $m = 2$ be a bounded domain with a connected boundary $\Gamma = \partial D_-$ and $\mathbf{n}$ the unit normal to Γ pointed to the exterior domain $D_+ = \mathbf{R}^m - \bar{D}_-$. The exterior Dirichlet problem is then cast as follows

$$\begin{cases} \triangle u + k^2 u = 0 & : \quad \text{in} \quad \mathrm{D}_+ \\ u = f & : \quad \text{on} \quad \Gamma \\ \frac{\partial u}{\partial r} - iku = o(r^{(1-m)/2}), & : \quad r = |\mathbf{x}| \to +\infty. \end{cases} \tag{1}$$

The solution is given, in the form of a combined double- and single-layer potential with a positive coupling parameter η, by

$$u(x) = \int_\Gamma \Big[\frac{\partial \Phi(x,y)}{\partial n(y)} - i\eta\Phi(x,y)\Big]\phi(y)ds(y), \qquad \mathrm{x} \in \mathbf{R}^{\mathrm{m}}\,\Gamma, \tag{2}$$

where the density ϕ is a solution of the integral equation

$$\phi + (K - i\eta S)\phi = 2f, \tag{3}$$

where $K, S : C(\Gamma) \to C(\Gamma)$ are defined by

$$(K\phi)(x) \equiv 2\int_\Gamma \frac{\partial \Phi(x,y)}{\partial n(y)}\phi(y)ds(y), \qquad \mathrm{x} \in \Gamma, \tag{4}$$

and

$$(S\phi)(x) \equiv 2\int_\Gamma \Phi(x,y)\phi(y)ds(y), \qquad \mathrm{x} \in \Gamma. \tag{5}$$

So far as inverse scattering problem is concerned, one is more interested in knowing the far-field pattern which is defined by the asymptotic behavior of the scattered wave

$$u(x) = \frac{e^{ik|\mathbf{x}|}}{\sqrt{|\mathbf{x}|}}\Big[u_\infty(\hat{\mathbf{x}}) + O\Big(\frac{1}{|\mathbf{x}|}\Big)\Big], \qquad |\mathbf{x}| \to +\infty, \tag{6}$$

where

$$u_\infty(\hat{\mathbf{x}}) = \frac{e^{-i\frac{\pi}{4}}}{\sqrt{8\pi k}} \int\limits_\Gamma \Big[\mathbf{k}\cdot\mathbf{n}(y,\hat{\mathbf{x}}) + \eta\Big] e^{-i\mathbf{k}\cdot\hat{\mathbf{x}}y} \varphi(y) ds(y). \tag{7}$$

III. ANALYSIS OF THE ALGORITHM

A fairly straightforward approach to attack the inverse scattering problem is described in the following steps.

(1) Guess a general shape of the obstacle:
Suppose that Γ is parametrized in two dimensions as a 2π-periodic function $R(\vartheta) \in C^2[0, 2\pi]$, where $\vartheta \in [0, 2\pi]$ is the polar angle. It is useful to represent $R(\vartheta)$ as a Fourier series

$$R(\vartheta) = \frac{a_0}{2} + \sum_{n=1}^{+\infty} \Big[a_n cos(n\vartheta) + b_n sin(n\vartheta)\Big], \tag{8}$$

where $\{a_n\}_{n=0}^{+\infty}$ and $\{b_n\}_{n\in\mathbf{N}}$ are Fourier coefficients. Regularity of Γ requires that $a_0 > 0$. The Fourier series formalism brings about essential convenience for analyzing the problem in a systematically tractable manner. The boundary Γ now is completely characterized by a sequence of Fourier coefficients $\mathbf{x} = (a_0, a_1, b_1, a_2, b_2, \ldots)$ as a vector in the parameter space, which is, in general, of infinite dimensions. In practice, however, given desired accuracy, it is sufficient to truncate such an infinite sequence at some certain order of harmonics.

To further illustrate this point, consider a simple example of two-dimensional scattering of a monochromatic wave off a trefoil-shaped obstacle whose boundary Γ is given by

$$R(\vartheta) = \frac{a_0}{2} + a_3 cos(3\vartheta), \tag{9}$$

where $a_0 = 2$ and $a_3 = 0.3$. The mission is to probe the shape of such presumably unknown obstacle by assuming that the angular power spectrum $|u_\infty^{meas}(\varphi)|^2$ is the only available information from measurements.

The most unexperienced algorithm to tiptoe in the parameter space would be routinary iterations by adding in one higher order harmonic component at a time to test if the results match. If the shape of the obstacle is well described by up to m^{th} order harmonics, then it takes no more than m iterations before termination. In particular, for the inverse scattering of a trefoil, it is enough to use merely the first three harmonics in which case $\mathbf{x} = (a_0, a_2, b_2, a_3, b_3) \in \mathbf{R}^5$. One may notice that the first harmonics, a_1 and b_1, have been excluded from the parameter sequence. This is because the absence of phase information in the angular power spectrum makes it immune to any rigid translational variation of the obstacle as a consequence of non-zero first harmonics [3].

Choosing the starting point of the search in the parameter space is rather deliberate. A good initial guess of $\mathbf{x}$ could pin down the shape of the obstacle with minimal amount of machine time whereas a bad initial guess could result in a failure in convergence or a false solution. Discussions of the arts of initial guessing and, more importantly, issues related to the uniqueness of inverse scattering problems are beyond the scope of the present paper. One is referred instead to more specialized literatures (e.g.[2]). What is shown in Section III though is a comparison of explicit examples of good initial guesses and bad ones for different wavelengths.

(2) Calculate the far-field pattern and the angular power spectrum $|u_\infty(\varphi, \mathbf{x})|^2$:
For a given vector $\mathbf{x}$ in the parameter space, one may follow standard recipes such as outlined in the previous section to solve for the far-field pattern and the angular power spectrum $|u_\infty(\varphi, \mathbf{x})|^2$.

(3) Minimize the error function with optimization:
The objective error function is defined as

$$f(\mathbf{x}) \equiv \| |u_\infty(\varphi, \mathbf{x})|^2 - |u_\infty^{meas}(\varphi)|^2 \|. \tag{10}$$

Finding the right shape of the obstacle now corresponds to minimizing $f(\mathbf{x})$ with respect to the vector $\mathbf{x}$ in the parameter space. Amongst a variety of minimum search algorithms, the simplex method is employed here as for reducing users' effort of evaluating $\nabla_\mathbf{x} f(\mathbf{x})$ at each iterative step. In addition, effective optimization is ubiquitously indispensable for any practical purposes. Numerically, for every fixed dimension of the parameter space, iterations should be terminated at some appropriately prescribed level of accuracy. The best case scenario would be that convergence to the true minimum ($\min_\mathbf{x} \mathrm{f}(\mathbf{x}) \sim 0$) is achieved and the shape of the obstacle ($\mathbf{x}_0$) is unveiled, with $f(\mathbf{x}_0) = \min_\mathbf{x} \mathrm{f}(\mathbf{x})$. As mentioned in (1), the initial guess could become a seriously critical factor in steering the search. On the other hand, the location of $\mathbf{x}_0$ is by no means perceptible, a priori, to any search algorithm with unbiased initial conditions. For parameter spaces with small dimensions, it may be helpful for narrowing down the hot zones in the landscape of minima by examining the dependence of the error function upon one or two parameters (see examples in Sec. III)

IV. NUMERICAL EXAMPLES

The inverse scattering of a trefoil-shaped obstacle in two dimensions is solved numerically in two different regimes–one with incident wave of a long wavelength ($k = 1$) and the other of a short wavelength ($k = 10$) in dimensionless units. In each case, both good and bad initial guesses are given in support of the analysis in Section II. Also presented are image and contour plots of the error functions in the $a_0 - a_3$ plane with

$a_2 = b_2 = b_3 = 0$ featuring a visually tangible recognition of the locations of $\mathbf{x}_0$ in each case. Even though they cannot substitute the search algorithm, these polts clearly are of significant assistance in choosing more rational initial guesses to start with.

(1) $k = 1$:

The measured angular power spectrum is shown in Fig. 1 Results from good and

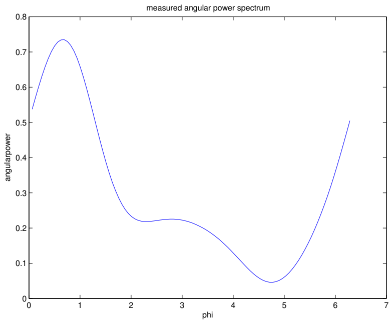

FIG. 1: The measured angular power spectrum $|u_\infty^{meas}(\varphi)|^2$ where φ is the scattering angle. The peak near $\varphi = 0$ coresponds to the major reflection of the incident wave from the front of the obstacle that is illuminated. The hump around $\varphi = \pi$ is the diffraction passing through the obstacle. The lack of details in the spectrum implies that the length scale of the obstacle is relatively small compared to the wavelength of the incident wave.

bad initial guesses are recorded in Table IV.

	Good	Bad
$\mathbf{x}_i$	(1.5, -0.2, 0.1, 0.2, -0.2)	(5.8, -0.5, 0.8, -2.2, 7.2)
$\mathbf{x}_0$	(2.000004735618671e+00,	(3.2293,
	-6.898564628619414e-08,	-1.3852,
	9.571497559335632e-07,	0.8384,
	3.000009317261063e-01,	-0.0698,
	-2.796144329369090e-06)	1.4777)
$f(\mathbf{x}_0)$	2.439251932922520e-06	0.4780
$\mathrm{N}_{\mathrm{iter}}$	330	411
$\mathrm{N}_{\mathrm{count}}$	533	705

With the good initial guess, the optimized angular power spectrum and its deviation from the measured one are shown in Fig. 2 and Fig. 3, respectively. In contrast, the angular power spectrum and its deviation from the measured one with the bad initial guess are shown in Fig. 4 and Fig. 5, respectively.

It is of considerable interest to examine the global distribution of the objective error function $f(\mathbf{x})$ in the parameter space. However, it is only feasible to plot the dependence of $f(\mathbf{x})$ upon two parameters at a time. For illustrative purposes, only the distribution on the hyperplane $(a_0, 0, 0, a_3, 0)$ is shown since a_0 and a_3 are the most relavant parameters in the trefoil scattering problem. Below are the image scale (Fig. 6) and contour (Fig. 7) plots of $f(\mathbf{x})$ with respect to (a_0, a_3).

(2) $k = 10$:

The measured angular power spectrum is

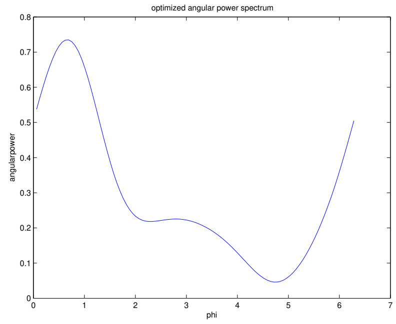

FIG. 2: The angular power spectrum yielded by the minimization routine with the good initial guess in Table IV.

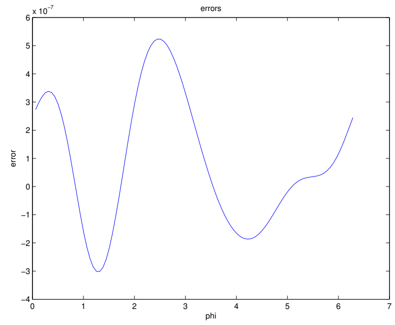

FIG. 3: The deviation of the angular power spectrum yielded by the minimization routine with the good initial guess in Table IV from the measured one. It is of the order 10^{-7}.

shown in Fig. 8 Results from good and bad initial guesses are recorded in Table IV.

Good	Bad	
$\mathbf{x}_i$	(1.0, -0.5, 0.3, 0.1, -0.2)	(4.0, -1.0, 0.7, -1.0,-0.5)
$\mathbf{x}_0$	(2.000,	(0.6370,
	-0.0000	-1.2902,
	0.0000,	0.7584,
	0.3000,	-1.2108,
	0.0000)	-0.6198)
$f(\mathbf{x}_0)$	1.9439e-05	7.6616
$\mathrm{N}_{\mathrm{iter}}$	353	386
$\mathrm{N}_{\mathrm{count}}$	565	626

With the good initial guess, the optimized angular power spectrum and its deviation from the measured one are shown in Fig. 9 and Fig. 10, respectively. In contrast, the angular power spectrum and its deviation from the measured one with the bad initial guess are shown in Fig. 11 and Fig. 12, respectively.

Similarly, the image scale (Fig. 6) and contour (Fig. 7) plots of $f(\mathbf{x})$ with respect to (a_0, a_3) are shown below.

It is worthwhile to point out, before ending this section, that vectorization of MatLab codes is also one of the key issues that can never be overlooked. With currently available computing facilities, inefficient vectorization or optimization could lead to an extraordinarily long com-

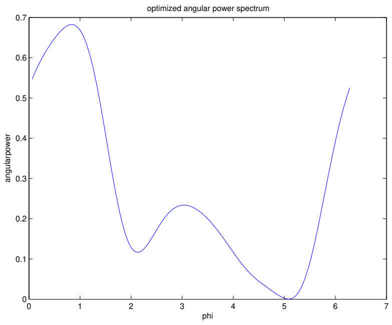

FIG. 4: The angular power spectrum yielded by the minimization routine with the bad initial guess in Table IV. It is way off from the measured one.

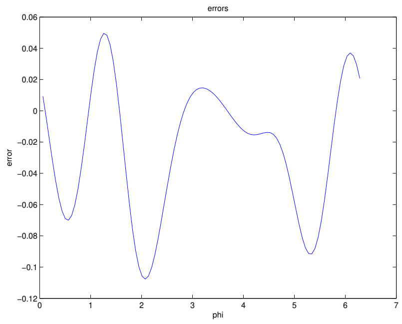

FIG. 5: The deviation of the angular power spectrum yielded by the minimization routine with the bad initial guess in Table IV from the measured one. It is obvious that the search routine has landed on some false or local minimum.

puting time.

V. SUMMARY AND DISCUSSIONS

The problem of inverse scattering of a two-dimensional solid obstacle with simple boundary in an otherwise spatially homogeneous unbounded region is solved. The parametrization of the boundary in terms of the Fourier series gives a parameter space containing Fourier coeffients up to a certain order of harmonics. Iterations over the vectors in such parameter space search for the minimum of the objective error function that corresponds to the correct shape of the unknown boundary. The method of boundary integral equations is adapted in the solution of exterior Dirichlet problem with given boundary shape characterized by the vectors in the parameter space.

It might improve the convergence speed and the robustness of the minimum search routine if additional constraints on the parameters that are compatible with the specific problem at hand are imposed throughout the iteration process. Moreoever, it would be intersting to explore how better accuracy could be attained if phase information in the scattered wave was included. These considerations will be left as future work.

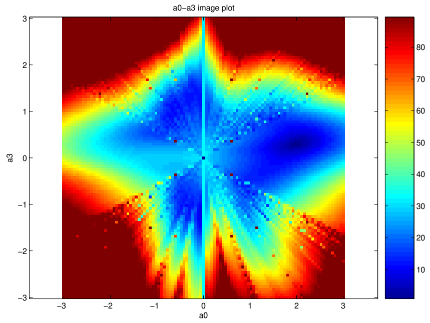

FIG. 6: Image-scale plat of the dependence of $f(\mathbf{x})$ upon two most relavant parameters a_0 and a_3 in the parameter space. It is clearly seen with the help of color bars that the true minimum is located at $(2.0, 0.3)$.

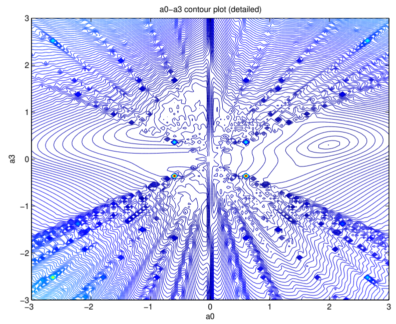

FIG. 7: Contour plots of the dependence of $f(\mathbf{x})$ upon two most relavant parameters a_0 and a_3 in the parameter space. It is clearly shown that the true minimum is located at $(2.0, 0.3)$.

Acknowledgments

I benefitted greatly from the lectures and interactions with the participants. I wish, in particular, to express my thanks to A. Barnett for his consistently overwhelming encouragement, most generous help with MatLab codes, and of course his guidance throughout the conduct of this project as well.

[1] R. Kress, Mathl. Comput. Modeling, **15**, 229 (1991).
[2] D. Colton and R. Kress, "Inverse acoustic and electromagnetic scattering theory", Springer-Verlag (1992).
[3] A. Barnett, private communication.

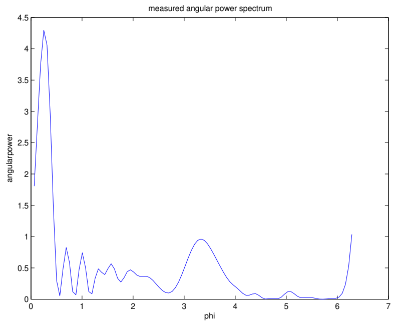

FIG. 8: The measured angular power spectrum $|u_\infty^{meas}(\varphi)|^2$ where φ is the scattering angle. The peak near $\varphi = 0$ coresponds to the major reflection of the incident wave from the front of the obstacle that is illuminated. The hump around $\varphi = \pi$ is the diffraction passing through the obstacle. The richer details in the spectrum implies that the length scale of the obstacle is now comparable to the wavelength of the incident wave. More information of the shape of the obstacle is encoded in the spectrum. However, it also becomes more challenging to extract the shape of the boundary as inverse scattering is concerned.

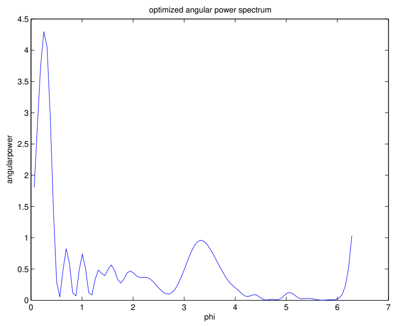

FIG. 9: The angular power spectrum yielded by the minimization routine with the good initial guess in Table IV.

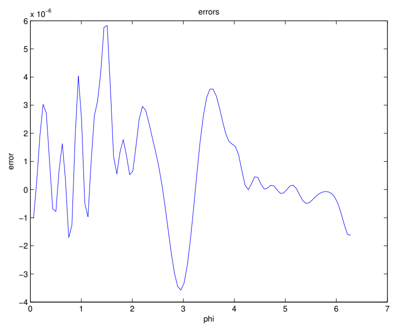

FIG. 10: The deviation of the angular power spectrum yielded by the minimization routine with the good initial guess in Table IV from the measured one. It is of the order 10^{-6}.

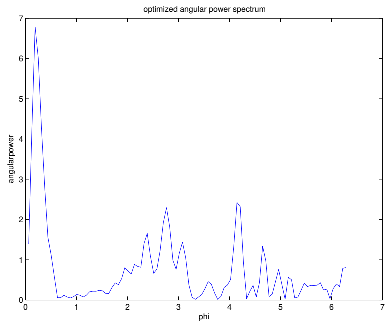

FIG. 11: The angular power spectrum yielded by the minimization routine with the bad initial guess in Table IV. It is way off from the measured one.

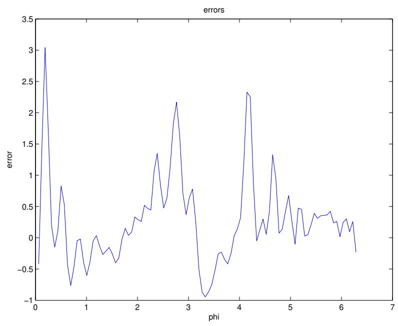

FIG. 12: The deviation of the angular power spectrum yielded by the minimization routine with the bad initial guess in Table IV from the measured one. It is obvious that the search routine has landed on some false or local minimum.

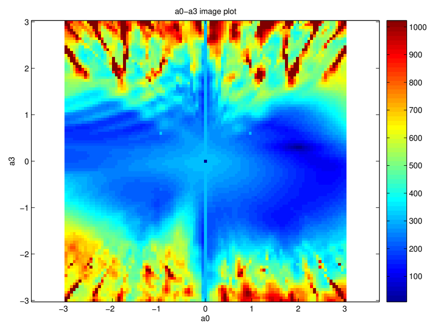

FIG. 13: Image-scale plat of the dependence of $f(\mathbf{x})$ upon two most relavant parameters a_0 and a_3 in the parameter space. It is clearly seen with the help of color bars that the true minimum is located at $(2.0, 0.3)$.

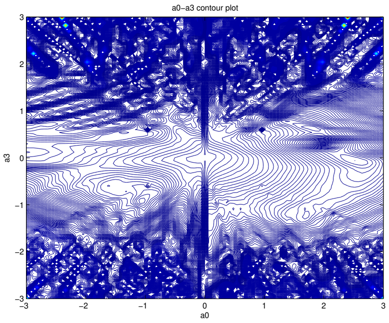

FIG. 14: Contour plots of the dependence of $f(\mathbf{x})$ upon two most relavant parameters a_0 and a_3 in the parameter space. It is clearly shown that the true minimum is located at $(2.0, 0.3)$.